08

Formation of germanium nanocrystals and amorphous nanoclusters in GeO[SiO] and GeO[SiO_2] films using electron beam annealing

© V.O. Konstantinov,[1] E.A. Baranov,[1] Zhang Fan,[2,3] V.G. Shchukin,[1] A.O. Zamchiy,[1,2] V.A. Volodin[2,3]

[1]Kutateladze Institute of Thermophysics, Siberian Branch, Russian Academy of Sciences,
630090 Novosibirsk, Russia
[2]Novosibirsk State University,
630090 Novosibirsk, Russia
[3]Rzhanov Institute of Semiconductor Physics, Siberian Branch, Russian Academy of Sciences,
630090 Novosibirsk, Russia
e-mail: konstantinov@itp.nsc.ru

Received February 9, 2022
Revised May 13, 2022
Accepted May 17, 2022

Electron beam annealing was carried out to form amorphous and crystalline germanium clusters in GeO[SiO] and GeO[SiO_2] films deposited on quartz and monocrystalline silicon substrates. Using electron microscopy, Raman spectroscopy, and light transmission and reflection spectroscopy, the structural transformations of the films and their optical properties were studied. From the analysis of Raman spectra, it was shown that amorphous germanium nanoclusters are present in the as-deposited GeO[SiO] film, while they are not observed in the as-deposited GeO[SiO_2] film. Regimes of electron beam annealing which are necessary for the formation of germanium nanocrystals in GeO[SiO] and GeO[SiO_2] films were found. It was shown that, at the same annealing parameters, the fraction of the crystalline phase of germanium in GeO[SiO] films were smaller than in GeO[SiO_2] films. In addition, it was found that the fraction of the crystalline phase at the same annealing parameters is larger for films on a quartz substrate than on monocrystalline silicon substrate. The sizes of germanium nanocrystals formed as a result of electron beam annealing were determined from Raman spectra analysis. The proposed method of obtaining amorphous germanium nanoclusters and nanocrystals in films of nonstoichiometric germanosilicate glasses using electron beam annealing can be used to create ordered arrays of such nanostructures.

Keywords: films of nonstoichiometric germanosilicate glass, electron beam annealing, germanium nanoclusters and nanocrystals.

DOI: 10.21883/TP.2022.09.54685.28-22

Introduction

Dielectric films containing amorphous germanium nanoclusters and nanocrystals (NC-Ge) are of interest from a fundamental point of view [1], and also promising for nano- and optoelectronics [1, 2]. For example, GeO_x films are applied as an anti-reflecting coating in solar cells [3]. The relevance of the application of germanosilicate films in nanoelectronics is due to their special electrical properties. It is known that the mobility of electrons and holes in germanium is greater than in silicon [4], but the breakdown voltages of germanium dioxide (GeO_2) are lower than those of silicon dioxide. Furthermore, GeO_2 has poor chemical resistance, and, as an example, it dissolves quite well in water. Therefore, germanium oxynitride [5] films or films with a high dielectric constant (high-*k* dielectrics) [6] are applied to create MIS transistors based on germanium. GeO_x or $GeSiO_x$ [7] layers act as a transition layer between Ge and a high-*k* dielectric film. Films of nonstoichiometric germanium oxides are also very promising for application in accumulator cell with an increased number of recharge cycles [8]. In addition to amorphous germanium oxides, $GeSiO_x$ oxides containing nanocrystals of Ge, Si and their solid solutions are used in photosensitive detector [9].

It is known that GeO_x and $GeSiO_x$ amorphous films are metastable, and as the temperature increases, there are disproportionation reactions occur $2GeO \rightarrow Ge+GeO_2$ [9,10] (in the case of GeO_1 films); $GeO+SiO \rightarrow Ge+SiO_2$ (in the case of $GeSiO_2$ films); $2GeO+2SiO_2 \rightarrow Ge+3Ge_{1/3}Si_{2/3}O_2$ (in the case of $GeSiO_3$ films) [11]. Furnace annealing [9–11] is usually applied for disproportionation and formation of amorphous nanoclusters and NC-Ge. However, the use of radiation exposure has a number of advantages, for example, it allows to create amorphous nanoclusters and nanocrystals (NC) in local areas of thin films, minimizing the thermal effect on the substrate. Previously, researchers [12] applied ion-beam annealing of GeO_x thin films with an energy of 150MeV Ag^+, which led to the formation of NC-Ge with a size of up to 30 nm. By now, abundant papers have been devoted to electron-- beam annealing of amorphous germanium films [13,14], and only one paper which was devoted to electron-beam annealing of nonstoichiometric germanosilicate glasses [15]. In this paper, electron beam annealing (EBA) was used to form amorphous germanium clusters and crystallize them in GeO[SiO] and GeO[SiO_2] films.

1. Experiment description

GeO[SiO] and GeO[SiO_2] thin films were obtained by the simultaneous evaporation of GeO_2 and SiO powders (or GeO_2 and SiO_2) using electron beams in high vacuum (10^{-6} Pa). The power of the electron beams that evaporated the targets was chosen so that the deposition rate of both components was the same. Meanwhile, it was previously obtained [9] that, upon evaporation of the GeO_2 target, a GeO_x layer is deposited with the stoichiometric parameter $x \sim 1$ on the substrate. According to the stoichiometric composition, which was studied in the paper [16], the films will be designated as GeO[SiO_2] (composition of $GeSiO_3$) and GeO[SiO] (composition of $GeSiO_2$). The films were deposited at a temperature of 100°C on fused quartz and *c*-Si (100) substrates. The thickness of the films was ~ 400 nm. The films were covered with a SiO_2 protective layer 10 nm thick to avoid evaporation of germanium monoxide during annealing [17].

Further, to anneal the as-deposited films, an electron beam generated by a discharge electron gun with a hollow cathode was used [18]. The current density of the electron beam was 20 mA/cm^2 at an accelerating voltage of 2000 V. The choice of the annealing mode parameters is due to the results from the article [19], where it is shown that for an electron beam with an accelerating voltage of 1000 V and a current of 100 mA, even at an annealing time of 600 s, polysilicon was not formed, and the action of an electron beam with an accelerating voltage of 3000 V and a similar current led to the evaporation of a-SiO_x:H thin film for 60 s. The sample surface area of electron beam irradiation beam was 0.3 cm^2. The samples were placed perpendicular to the electron beam in a vacuum chamber with a pressure of 10^{-2} Pa. The time of annealing was 60 s and it was controlled by turning the electron gun on and off.

The electron microscopy was applied to analyze the structure of the films. A JEM-2200FS microscope with an accelerating voltage of 200 kV was used in the high-resolution transmission electron microscope (HRTEM) mode. The preparation of samples for HRTEM studies in cross-section consisted in the following: these samples on a c-Si (100) substrate were thinned by mechanical polishing using a Leica EM TXP microscope, followed by final thinning with an ion beam. The elemental composition of the films was analyzed in the course of microscopic studies using the energy dispersive X-ray spectroscopy (EDX, EDRS, or EDS) method.

The structure of the films was analyzed using Raman spectroscopy. The Raman spectra were recorded in backscattering geometry using T64000 spectrometer (Horiba Jobin Yvon) with Ar^+ laser ($\lambda = 514.5$ nm) excitation, the spectral resolution was no worse than 2 cm^{-1}. All spectra were measured at room temperature; no local heating of the films by laser radiation occurred during the recording of the spectra.

The transmission and reflection spectra of the films were studied using an SF-56 spectrophotometer (LOMO-Spektr, St. Petersburg). The spectral resolution was 2 nm, the measurement range was from 190 to 1100 nm. Reflection spectra were recorded using a specular reflection attachment; the angle of incidence was 9° from the normal. As a reference spectrum, the reflection spectrum from silicon with a natural oxide 3 nm thick was applied, the reflection spectrum of the film under study was multiplied by the reference spectrum.

2. Results and discussion

According to the EDS analysis, the films contain germanium, silicon and oxygen. The distribution results of germanium over the film thickness are shown in Fig. 1. In the as-deposited GeO[SiO] film, the germanium atoms are almost uniformly distributed over the film thickness (Fig. 1, *a*), and after annealing, a 15% increase in germanium concentration was observed in the 100 nm thick layer bordering the silicon substrate in the film (Fig. 1, *b*). A similar effect of germanium drift to the substrate was observed earlier during furnace annealing of multilayer GeO/SiO_2 [20] structures.

The formation of NC-Ge in the GeO[SiO] film after EBA was detected by direct electron microscopy. Figure 2 presents HRTEM image of a GeO[SiO] film on Si substrates after EBA. The image demonstrates NC-Ge, amorphous germanium clusters, and a glassy matrix. The average size of NC-Ge is approximately 5.5 nm, and the average size of amorphous nanoclusters is approximately 6 nm. Previously, it was shown that the as-deposited film did not contain NC-Ge [21].

Figure 3 presents the Raman spectra of GeO[SiO] and GeO[SiO_2] films deposited on a silicon substrate before and after annealing. To monitor over the structural transformations of the films after EBA, the spectra of the as-deposited films were the first to be recorded (black curves in Fig. 3). The spectra of the as-deposited films contain an intense narrow peak ~ 520.5 cm^{-1} associated with scattering by long-wavelength optical phonons from the c-Si substrate. In the spectrum of the as-deposited film in Fig. 3, *b* there is also a very weak feature ~ 305 cm^{-1} associated with two-phonon scattering by transverse acoustic phonons in the silicon substrate, which indicates that the films are translucent to green light. The spectrum of the as-deposited GeO[SiO] film (Fig. 3, *a*) shows a broad peak ~ 275 cm^{-1}, which is associated with the presence of amorphous germanium clusters, this is scattering on local vibrations of Ge-Ge bonds in amorphous germanium [22]. This is due to the fact that during the deposition at the temperature of 100°C, the oxide-reduction reaction GeO+SiO→SiO_2+Ge(amorphous) occurred [23]. It can be seen that, after EBA the amorphous germanium clusters have partially crystallized (red curve (in the online version), Fig. 3, *a*). When the spectrum was decomposed into Gauss curves, it was discovered that the position of the „nanocrystalline“ peak is ~ 299.9 cm^{-1}, while a wide „amorphous“ peak remains in the spectrum.

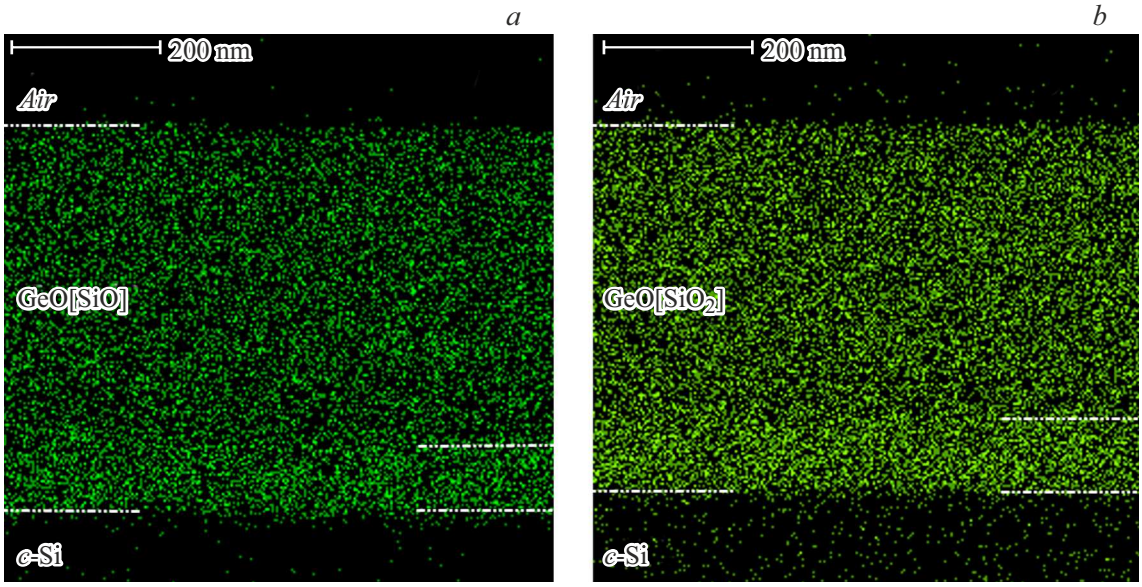

Figure 1. Distribution of germanium in a GeO[SiO] film on a silicon substrate obtained from EDS data analysis: *a* — initial film, *b* — film after EBA.

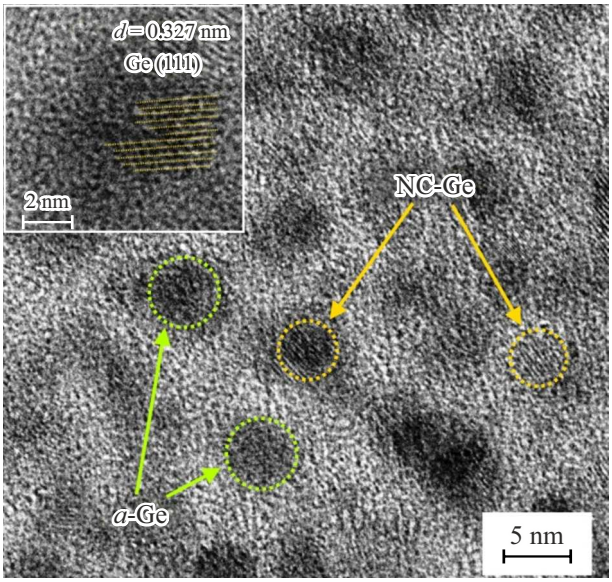

Figure 2. Dark-field HRTEM images of a GeO[SiO] film on a *c*-Si (001) substrate after EBA.

Neither „amorphous“nor „nanocrystalline“ germanium peaks were found in the spectrum of the as-deposited $GeO[SiO_2]$ film. It is likely, this film does not contain sufficiently large germanium clusters. It can be seen that after EBA, the spectrum is dominated by a narrow peak with the position $\sim 300.0\,cm^{-1}$ (red curve (online version), Fig. 3, *b*), but decomposition into peaks showed that there is also an „amorphous“ peak, i.e. both crystalline and amorphous phases of germanium are present.

Proceeding to the analysis of the Raman spectra of GeO[SiO] and $GeO[SiO_2]$ films on quartz substrates (Fig. 4). As can be seen, the Raman spectrum of the as-deposited GeO[SiO] film on quartz (black curve, Fig. 4, *a*) contains a signal from amorphous germanium clusters (the above-mentioned peak at $\sim 275\,cm^{-1}$). To analyze the effect of current density homogeneity in the electron beam after EBA, several spectra were recorded. Point p_1 — is a point in the center of the beam, and point p_5 — is on the edge of the beam, points p_2-p_4 — are intermediate points that are at equal distance from each other. Recall that the beam diameter was 6 mm, and its radius was 3 mm, respectively. It can be seen that EBA at the center of the beam (point p_1) led to almost complete crystallization of amorphous germanium clusters with the formation of NC-Ge, while the position „of the nanocrystalline“ peak was $\sim 303.8\,cm^{-1}$ (red curve (online version), Fig. 4, *a*). With a shift from the center of the beam, there is a shift of the peak position towards lower frequencies, while an „amorphous“ component appears in the spectra, this is especially noticeable in the spectrum recorded near the edge of the electron beam (point p_5 — violet curve, Fig. 4, *a*).

The spectrum of the as-deposited $GeO[SiO_2]$ film (Fig. 4, *b*) contains features associated with the signal from the quartz substrate (a wide band from 250 to $550\,cm^{-1}$ and a feature at $\sim 495\,cm^{-1}$). As noted previously, this is due to the fact that this film is semitransparent at the laser wavelength (i.e., the laser light reaches the substrate). Thus, it has been shown that, in the as-deposited $GeO[SiO_2]$ film on a quartz substrate, there are no clusters of amorphous and crystalline germanium.

From the analysis of the spectrum from the point p_1 (red curve (online version), Fig. 4, *b*) it can be seen that the EBA at the center of the beam led to the formation of NC-Ge in the $GeO[SiO_2]$ film on the quartz substrate. When the spectra were decomposed into Gauss curves,

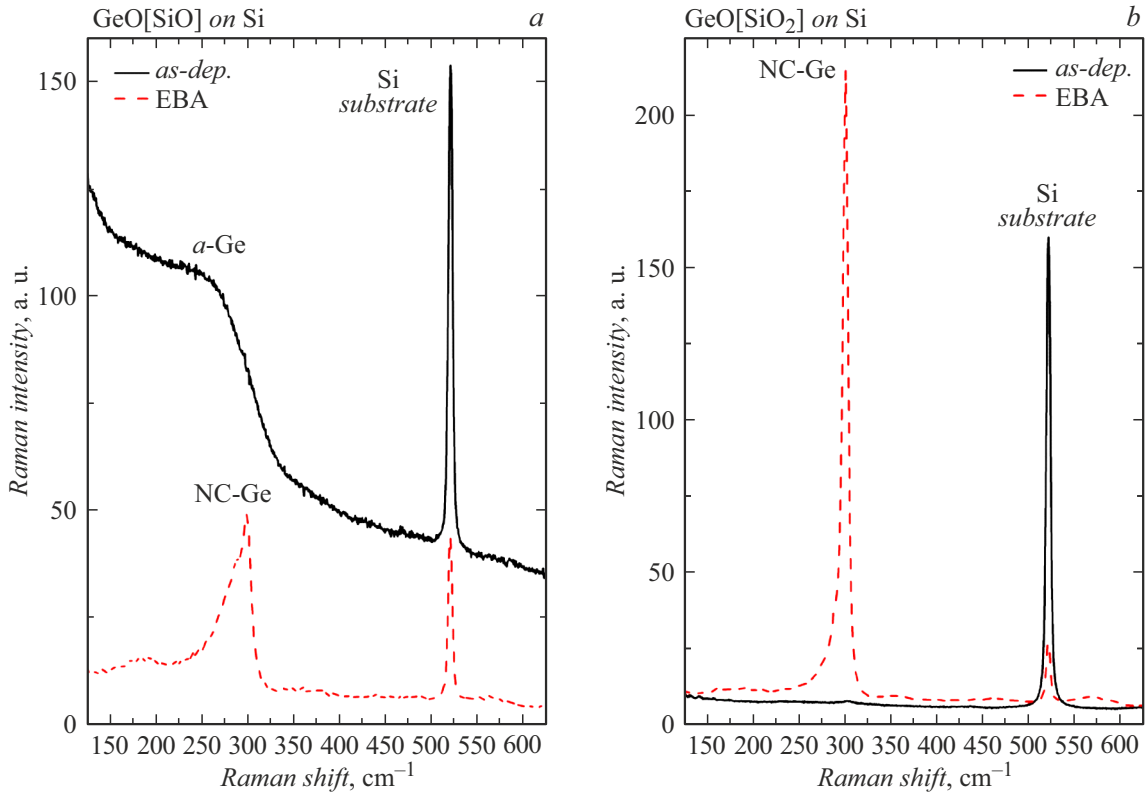

Figure 3. Raman spectra of films on silicon substrates: *a* — GeO[SiO], b — GeO[SiO_2].

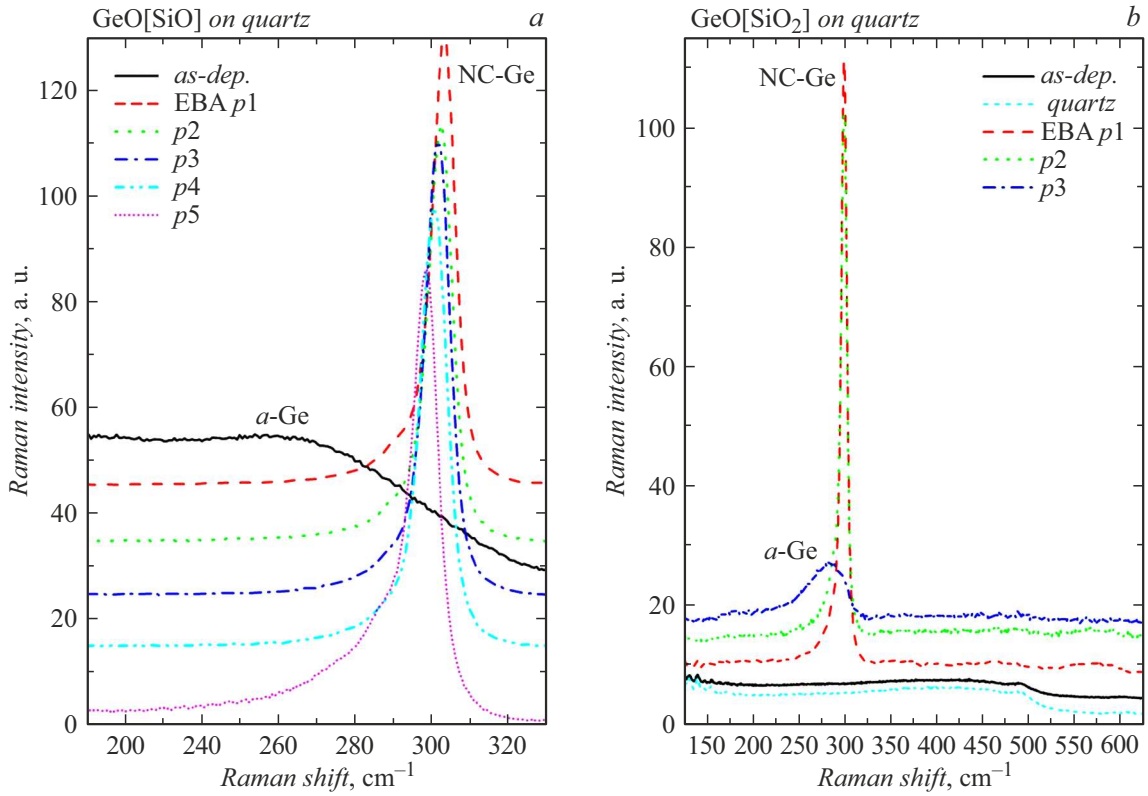

Figure 4. Raman spectra of films on quartz substrates: *a* — GeO[SiO], *b* — GeO[SiO_2].

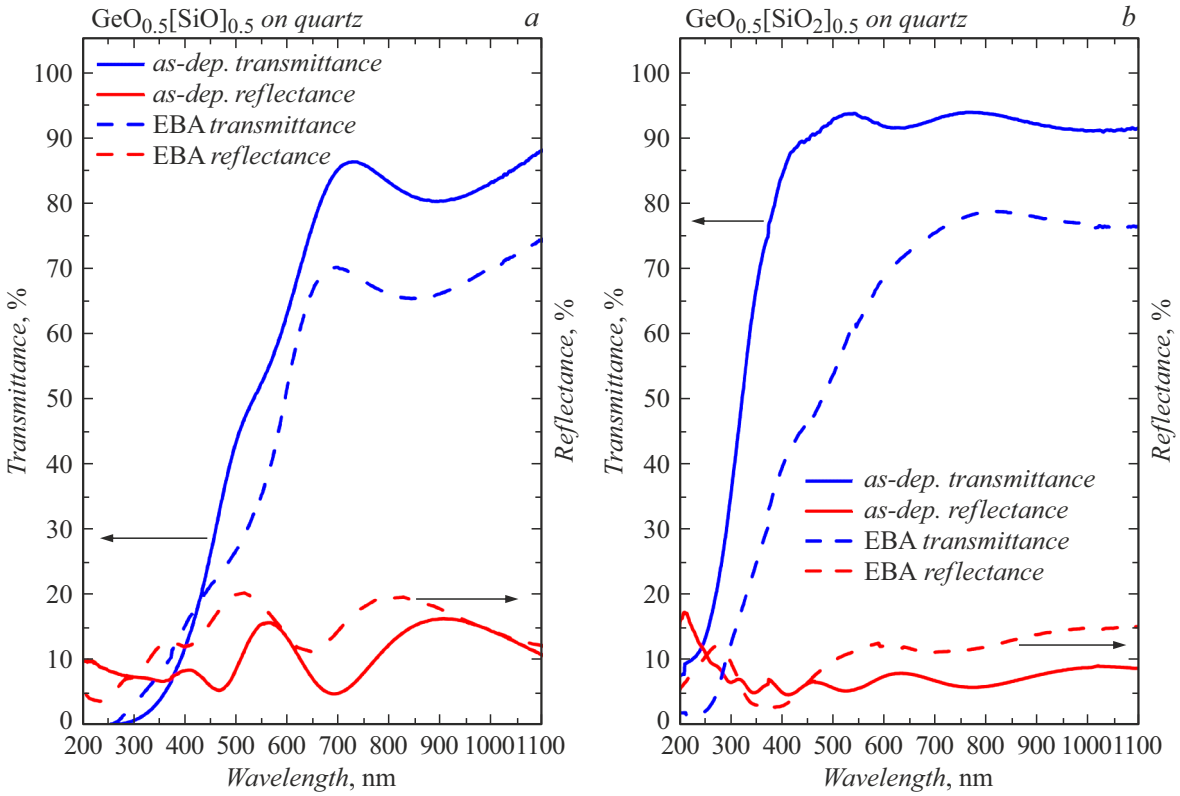

Figure 5. Transmission and reflection spectra of films on quartz substrates: *a* — GeO[SiO], *b* — GeO[SiO_2].

the position of the peak from NC-Ge was obtained, which is 299.3 cm^{-1}, while the „amorphous“ component of the peak is insignificant. The influence of the current density homogeneity in the electron beam was analyzed as well. It can be seen that at the point p_2 (green curve (online version), Fig. 4, *b*) located in the middle between the center of the beam and its edge, the Raman spectrum is almost indistinguishable from the spectrum at the point p_1 (beam center). A in the spectrum from point p_3 (beam edge, blue curve (online version), Fig. 4, *b*), „amorphous“ peak dominates. Obviously, the observed results are due to the decrease in the current density in the electron beam from its center to the edge.

Figure 5 presents the transmission and reflection spectra of GeO[SiO] and GeO[SiO_2] films before and after EBA.

It can be seen that EBA led to a decrease in the transparency of the films, this is especially evident from the shift of the absorption edge for the GeO[SiO_2] film. This is due to the formation of amorphous clusters and NC-Ge in the films, which leads to the absorption of visible and IR radiation [11].

3. Analysis of obtained results

Previously, the authors showed that the as-deposited GeO[SiO] film contains amorphous germanium nanoclusters with an average size of ~ 3 nm [21]. EBA led to the formation of NC-Ge in this film. There were no germanium clusters in the as-deposited GeO[SiO_2] film; after EBA, NC-Ge were also formed in it. The table shows the average size of NC-Ge and the volume fraction of the crystalline phase, which were determined from the analysis of the Raman data.

The comparison of the GeO[SiO_2] and GeO[SiO] films after annealing presents that the fraction of the crystalline phase in the GeO[SiO_2] film is higher. Previously, the authors discovered that in the case of furnace annealing of such NC-Ge germanium films, the formation in the GeO[SiO_2] film begins already after a half-hour annealing of 550°C, whereas for the beginning of crystallization for amorphous germanium clusters in a GeO[SiO] film, annealing of the same duration at a temperature of 680°C [11] was required. This is due to the fact that the sizes of amorphous germanium clusters in the as-deposited GeO[SiO] film are smaller than the sizes of amorphous germanium clusters formed in the GeO[SiO_2] film due to the disproportionation reaction $2GeO+2SiO_2 \rightarrow Ge+3Ge_{1/3}Si2/3O_2$ as a result of annealing [21]. It is known that the crystallization of large amorphous clusters in a refractory matrix occurs at a higher rate than the crystallization of small clusters.

It should be noted that, in the case of a quartz substrate, crystallization occurs at lower annealing parameters than in the case of a single-crystal silicon substrate. Most likely, this is due to the different thermal conductivity of these materials. This fact suggests that EBA leads to a thermal

Phase composition of germanium nanoclusters and the average size of NC-Ge

Sample	Annealing		Difference of NC peak position and peak from single-crystal size of NC Ge, cm^{-1}	Average nm	Fraction of crystal-lithyc phase, %
GeO[SiO]	As-deposited		–	–	0
	EBA	Quartz, point *1*	−1.78	–	100
		Quartz, point *2*	−0.9	–	100
		Quartz, point *3*	−0.21	–	100
		Quartz, point *4*	0.77	8	55
		Quartz, point *5*	2.84	4.5	55
		Si	1.51	6.2	10
GeO[SiO_2]	As-deposited		–	–	–
	EBA	Quartz, point *1*	2.13	5.3	53
		Quartz, point *2*	2.28	5.1	100
		Quartz, point *3*	–	–	0
		Si	1.42	6.4	50

effect, this is obvious, since the electron energy is too low for radiative effects.

Some differences between the NC-Ge dimensions obtained from the analysis of Raman data (see the table) and from the analysis of the HRTEM image was specified, which may be due to mechanical stresses in NC-Ge. Compression stresses result in an increase in phonon frequencies. According to the phonon localization model [24], with an average size of NC-Ge of 5.5 nm (the size from the HRTEM data), the difference in the positions of the peaks from NC-Ge and *c*-Ge should be 1.96 cm^{-1}, while according to the experiment it is 1.51 cm^{-1}. The difference of 0.45 cm^{-1} can be caused by compression stresses of 200−300 MPa [25]. It should also be noted that the peak frequency from NC-Ge is higher than from *c*-Ge for the GeO[SiO] film on quartz after EBA (points *1*−*3*). In this case, the NC-Ge are clearly subjected to mechanical compression, and their sizes cannot be determined from the analysis of the Raman spectra. The occurrence of mechanical compression stresses has already been detected after the complete crystallization of SiO_x films using EBA [19]. The reasons for the occurrence of such stresses and their influence on the crystallization kinetics have not yet been specified and will be the subject of further research.

The proposed approach to the formation of amorphous germanium and NC-Ge nanoclusters using an electron beam can be used to create layer-ordered amorphous nanoclusters and NC-Ge. However, for this it is required to use an electron beam of higher energy, i.e. to use not thermal, but radiation effects for structural transformations in films. For nanometer resolution, it is required to use a focused electron beam, for example, as in an electron beam nanolithography. To create periodic arrays of amorphous nanoclusters and NC-Ge, the interference of monochromatic coherent electron beams can be applied, as proposed in [15].

Conclusion

The analysis of the Raman spectra showed that amorphous germanium nanoclusters are present in the as-deposited GeO[SiO] film, while they are not in the as-deposited GeO[SiO_2] film. It has been found that the use of electron beam annealing leads to the formation of amorphous and crystalline germanium nanoclusters in these films. The effects on the influence of the substrate (quartz or silicon), as well as the composition of the films, on the size of germanium nanocrystals and the fraction of the crystalline phase (in the case of incomplete crystallization of germanium clusters) as a result of electron beam annealing have been studied. The influence of current homogeneity in an electron beam on structural transformations has been studied.

Acknowledgments

The authors express their gratitude to Krivyakin G.K. for HRTEM measurements; as well as to the CUC of „VTAN“ Central Research Center for the provided equipment for recording Raman spectra and obtaining HRTEM images. The authors express their gratitude to Michel Vergnat (Université de Lorraine, France) for assistance in the increase of the initial films of nonstoichiometric germanosilicate films.

Funding

These studies were supported financially by the Ministry of Science and Higher Education of the Russian Federation. The work on electron-beam annealing was carried out under state assignment of IT SB RAS, project № 121031800218-5. The work on the study of the structure of the films was carried out according to the state order of the Institute of Physics of Semiconductors of the SB RAS, project № FWGW-2022-0011.

Conflict of interest

The authors declare that they have no conflict of interest.

References

[1] E.G. Barbagiovanni, D.J. Lockwood, P.J. Simpson, L.V. Goncharova. Appl. Phys. Rev., 1, 011302 (2014). DOI: 10.1063/1.4835095
[2] D. Carolan. Prog. Mater Sci., **90**, 128 (2017). DOI: 10.1016/J.PMATSCI.2017.07.005
[3] V.G. Dyskin, M.U. Dzhanklych. Appl. Sol. Energy, **57**, 252 (2021). DOI: 10.3103/S0003701X2103004X
[4] S.M. Sze. *Physics of Semiconductor Devices*, 2nd ed. (Wiley, NY., 1981), p. 789.
[5] Y. Minoura, A. Kasuya, T. Hosoi, T. Shimura, H. Watanabe. Appl. Phys. Lett., **103**, 033502 (2013). DOI: 10.1063/1.4813829
[6] Y. Kamata. Mater. Today, **11**, 30 (2008). DOI: 10.1016/S1369-7021(07)70350-4
[7] M. Shang, X. Chen, B. Li, J. Niu. ACS Nano, **14**, 3678 (2020). DOI: 10.1021/acsnano.0c00556
[8] I. Stavarache, C. Logofatu, M.T. Sultan, A. Manolescu, H.G. Svavarsson, V.S. Teodorescu, M.L. Ciurea. Sci. Rep., **10**, 3252 (2020). DOI: 10.1038/s41598-020-60000-x
[9] M. Ardyanian, H. Rinnert, M. Vergnat. J. Appl. Phys., **100**, 113106 (2006). DOI: 10.1063/1.2400090
[10] S.K. Wang, H. Liu, A. Toriumi. Appl. Phys. Lett., **101**, 2 (2012). DOI: 10.1063/1.4738892
[11] F. Zhang, S.A. Kochubey, M. Stoffel, H. Rinnert, M. Vergnat, V.A. Volodin. Semiconductors, **54** (3), 322 (2020). DOI: 10.1134/S1063782620030070
[12] Sh. Rath, D. Kabiraj, D.K. Avasthi, A. Tripathi, K.P. Jain, Manoj Kumar, H.S. Mavi, A.K. Shukla. Nucl. Instrum. Methods Phys. Res. Sect. B, **263**, 419 (2007). DOI: 10.1016/j.nimb.2007.07.018
[13] M. Okugawa, R. Nakamura, H. Numakura, M. Ishimaru, H. Yasuda. J. Appl. Phys., **120**, 134308 (2016). DOI: 10.1063/1.4964332
[14] R. Nakamura, A. Matsumoto, M. Ishimaru. J. Appl. Phys., **129**, 215301 (2021). DOI: 10.1063/5.0052142
[15] F. Zhang, V.A. Volodin, E.A. Baranov, V.O. Konstantinov, V.G. Shchukin, A.O. Zamchiy, M. Vergnat. Vacuum, **197**, 110796 (2022). DOI: 10.1016/j.vacuum.2021.110796
[16] V.A. Volodin, P. Geydt, G.N. Kamaev, A.A. Gismatulin, G.K. Krivyakin, I.P. Prosvirin, I.A. Azarov, F. Zhang, M. Vergnat. Electron MDPI, **9**, 2103 (2020). DOI: 10.3390/electronics9122103
[17] S.R.M. da Silva, G.K. Rolim, G.V. Soares, I.J.R. Baumvol, C. Krug, L. Miotti, F.L. Freire, Jr., M.E.H.M. da Costa, C. Radtke. Appl. Phys. Lett., **100**, 191907 (2012). DOI: 10.1063/1.4712619
[18] V.G. Shchukin, V.O. Konstantinov, V.S. Morozov. Tech. Phys., **63** (6), 888 (2018). DOI: 10.1134/S1063784218060191
[19] E.A. Baranov, V.O. Konstantinov, V.G. Shchukin, A.O. Zamchiy, I.E. Merkulova, N.A. Lunev, V.A. Volodin. Tech. Phys. Lett., **47**, 287 (2021). DOI: 10.1134/S1063785021030172
[20] V.A. Volodin, M.P. Gambaryan, A.G. Cherkov, M. Stoffel, H. Rinnert, M.Vergnat. Mater. Res. Express, **3**, 085019 (2016). DOI: 10.1088/2053-1591/3/8/085019
[21] M.P. Gambaryan, G.K. Krivyakin, S.G. Cherkova, M. Stoffel, H. Rinnert, M. Vergnat, V.A. Volodin Phys. Solid State, **62** (3), 492 (2020). DOI: 10.1134/S1063783420030105]
[22] W. Wihl, M. Cardona, J. Tauc. J. Non-Cryst. Solids, **8–10**, 172 (1972). DOI: 10.1016/0022-3093(72)90132-9
[23] V.A. Volodin, G.N. Kamaev, V.A. Gritsenko, A.A. Gismatulin, A. Chin, M. Vergnat. Appl. Phys. Lett., **114**, 233104 (2019). DOI: 10.1063/1.5079690
[24] V.A. Volodin, D.V. Marin, V.A. Sachkov, E.B. Gorokhov, H. Rinnert, M. Vergnat. JETF, **145**, 77 (2014). DOI: 10.7868/S0044451014010076
[25] F. Cerdeira, C.J. Buchenauer, F.H. Pollak, M. Cardona. Phys. Rev. B, **5**, 580 (1972). DOI: 10.1103/PhysRevB.5.580